Engineering Failure Analysis 16 (2009) 281–294

Contents lists available at ScienceDirect

Engineering Failure Analysis

journal homepage: www.elsevier.com/locate/engfailanal

Rail base corrosion problem for North American transit systems

F.C. Robles Hernández [a,*], G. Plascencia [b], Kevin Koch [a]

[a] Transportation Technology Center Inc. (TTCI), Pueblo 81001, USA
[b] CIITEC, Instituto Politécnico Nacional, México, DF, Mexico

ARTICLE INFO

Article history:
Received 18 March 2008
Accepted 27 May 2008
Available online 10 June 2008

Keywords:
Corrosion
Transit systems
Rail steels
Finite element analysis
DC current

ABSTRACT

This paper addresses the results of the microstructure and numerical simulation and corrosion analysis and effects of return (DC) current. The results of this research indicate that rail base corrosion can shorten rail's life from several decades to one year or less compromising integrity and transit system safety. Rail base corrosion is characteristic of rails located in tunnels or wet undergrounds. Rail base corrosion is the result of a combination of factors including humidity, accumulated salts at tie plates and clips, but most importantly the return current (DC) from the transit car traction motors. These factors promote galvanic reactions that increase corrosion rate of the rail. Perhaps the amount of rail lost due to corrosion is no more than 0.005% (6.5 kg km^{-1} $year^{-1}$) this apparently does not represent a major concern; however, rail base corrosion initiates and propagates by the local removal of the rail forming intricate shapes that act as stress concentrator reducing fatigue life performance. Under extreme circumstances a few grams of lost rail in the right location, with the right geometry and orientation can be responsible for its removal or failure shortening rail's life to less than a year and can compromise safety. The use of plastic ties and a return stray current system seem to be the most suitable solution for rail base corrosion.

1. Introduction

Rail base corrosion can represent a dangerous condition for track integrity and, eventually to the safety of transit systems. Rail base corrosion is commonly found in areas that lack ventilation and usually at locations with water leaks from drainage systems, lakes, and seas and other sources of water. One particular source of contamination for transit systems located along the US east coast is the salt (rich in chlorine and sulfates) used during the winter season to melt ice or snow from streets. Such salt dissolves in water and are carried over into drainage systems. When the salt and humidity combine with the return DC current that strays to ground, galvanic corrosion between the rail and tie plate is initiated, resulting in an aggressive environment that increases corrosion rates which are further enhanced by the high returning voltage and current [1,2].

Rails in transit systems are used to carry two types of currents: return current (usually DC) [4,7] and signal current (AC) [8,9]. AC current does not present a major concern for corrosion. In fact, most publications focusing on AC current discuss the effects of the conductance and resistance of the rail and the ground and their effects on signal system. There are a limited number of documents in the literature that discuss rail base corrosion [4–9]. One of the works published on rail base corrosion [6] proposes a method to control stray currents and was implemented with good results. The stray DC current control system lowers the density of stray current (thus corrosion) along the rail considerably and the stray current control system works as a sacrificial anode, second return current system on insulated rails to further reduce the effects of corrosion.

* Corresponding author. Tel.: +1 719 585 1852.
E-mail address: francisco_robles@aar.com (F.C. Robles Hernández).

1350-6307/$ - see front matter © 2008 Elsevier Ltd. All rights reserved.
doi:10.1016/j.engfailanal.2008.05.011

In addition, corrosion is generally hidden under the base and flanges of the rail, growing internally and forming intricate shapes within the flange impeding visual or ultrasonic inspection [4]. Based on the results reported by TTCI, average premium rail life in freight rail service is curves of approximately 2° or more is approximately 1500 million gross metric tons (MGMT), when based solely on wear [5]. If this rail performance could be realized on the North American transit systems, rails could last a few decades [10]. In extreme cases, rail's life in some transit systems environments is shortened to less than a year due the presence of corrosion representing an expensive, but most importantly, unsafe conditions [4].

The present work provides the results of the rail base corrosion analysis conducted on rails donated by various North American transit systems (including Canada, Mexico, and the United States). The main objective of this work is to demonstrate by means of finite element analysis (FEA) and induced corrosion tests followed by metallographic evaluation the severity of rail base corrosion and to determine the typical corrosion rates under different conditions. All other data used for this paper was either provided by the respective transit authorities or obtained from the transit literature [3,11–14].

2. Experimental

2.1. Metallographic sample preparation

Metallographic sample preparation was conducted following standard grinding and polishing procedures. The samples were prepared metallographically to compare the microstructure among the different rail locations in the vicinity of corroded areas and away from these areas, such as in the head of the rail. After the initial metallographic inspection, the samples were etched with a Nital 4 solution to reveal the microstructure.

2.2. Numerical simulations

The FEA model was conducted using two representative samples exhibiting the most common types of rail base corrosion conditions. The first rail sample, identified as 115-lb/yd rail, was donated by the Toronto transit commission (TTC-Toronto) and the second rail sample, identified as 136-lb/yd rail, was donated by AMTRAK-NY. Both of these rails were presumably located at a tie plate and in the presence of stray DC currents. The 115-lb/yd and 136-lb/yd rail designation represent rail geometry profiles (dimensions), as indicated by AREMA Chapter IV [15]. The FEA modeling was conducted using ANSYS software.

2.3. Corrosion analysis

The corrosion tests were carried out by applying ±20 mV to the corrosion potential of the reference electrode. In these tests, a silver–silver chloride electrode was used as reference electrode. The corrosion potential of such electrode is +799 mV with respect to the normal Hydrogen electrode at 25 °C.

The corrosion tests were conducted in different electrolytes (1 M KCl, 0.1 M KCl, 1 M Na_2SO_4 and 0.1 M Na_2SO_4), such electrolytes were chosen after reviewing the analysis of the soils from the US and Canada donated by transit systems [12]. It should be mentioned that the aim of the corrosion tests was to evaluate the effect of ions such as SO_4^{2-} and Cl^- on the corrosion resistance of the rails. The effect of such ions on the corrosion resistance of the rails are of importance due to the fact that soils across North America contain considerable amounts of sulfates (SO_4^{2-}) and chlorines (Cl^-). The experimental set up for the corrosion tests consisted of an electrolytic cell attached to a potentiostat – galvanostat apparatus, which is connected to a CPU through a data acquisition system. The potentiostat used in our tests is an EG & G Princeton Applied Research apparatus model 273. This equipment has a built in corrosion software M352 which enables to automatically run the corrosion experiments while it collects data and stores it in the CPU. Fig. 1 shows the experimental set up and the probes used in the corrosion tests.

3. Results and discussions

3.1. Corrosion mechanisms

Corrosion is defined as the deterioration of a material due to its interaction with its environment [1]. Corrosion is affected by several factors; namely electrochemical, metallurgical and environmental (Fig. 1). The formation of hydrochloric acid (HCl) is explained in the reactions shown in Fig. 2 as the result of the electrolytic decomposition of sodium chlorine (NaCl), potassium chlorine (KCl), and other chlorines in the presence of water. Sulfates, such as sodium sulfate (Na_2SO_4) or ammonium sulfate $(NH_4)_2SO_4$, are also decomposed, leading to sulfuric acid (H_2SO_4). The resultant hydrochloric and sulfuric acids form electrolytes, increase the corrosion rates promoting galvanic corrosion. The chemical composition of the salts deposited along the rail's base and flange contain chlorines and sulfates as previously reported [4,5].

Rust is formed when iron compounds corrode in the presence of oxygen and water, forming iron oxides and hydroxides. The process of rust formation can be summarized in three stages: (1) formation of Fe^{2+} [2,3] formation of hydroxide ions, and [3] the chemical reaction with oxygen to create rust. Hence, rust is Fe^{3+} oxide that is formed by the dehydration of Fe^{2+} and

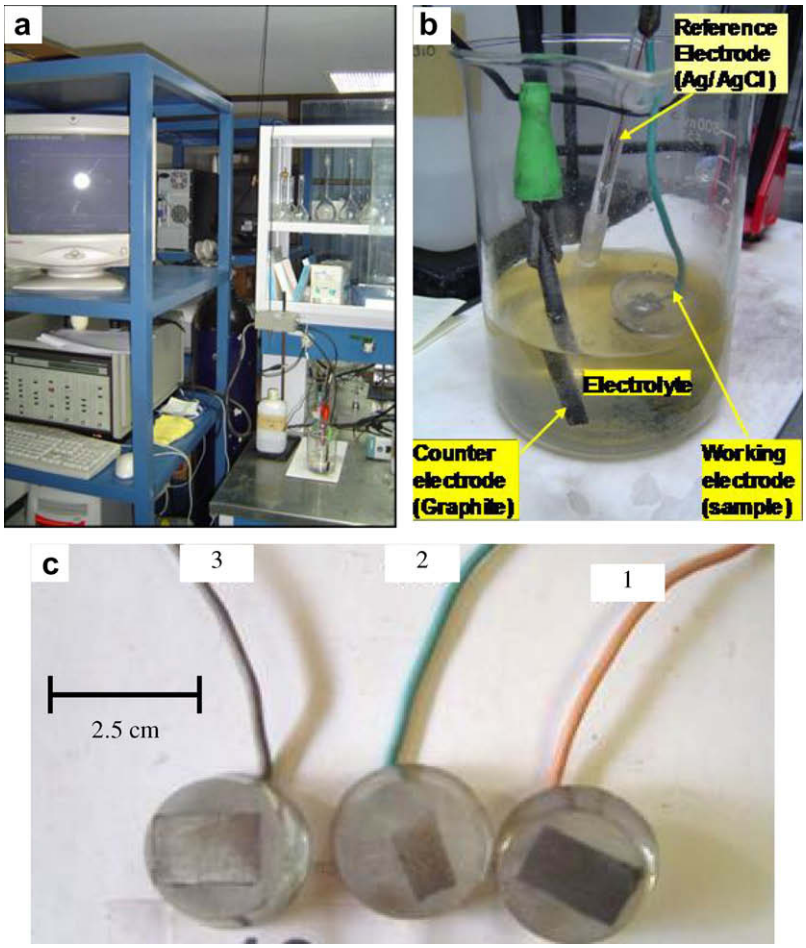

Fig. 1. (a and b) Experimental set up for corrosion tests and (c) probes used for corrosion testing. The picture shows the probes after being corroded in 0.1 M KCl electrolyte.

hydroxide. The concentration of chlorine ions accelerates corrosion by making the solution (water + salts) more conductive. A magnetic hydrous ferrite, $Fe_3O_4xH_2O$, often forms a black intermediate layer between hydrous Fe_2O_3 and FeO. Hence, rust films normally consist of three layers of iron oxides in different states of oxidation as shown in Fig. 2b [2,3].

3.2. Metallographic observations

Fig. 2 shows a rail installed in an underground location that was removed due to excessive corrosion. The polished samples from this rail were analyzed using optical microscopy and stereography techniques to verify their microstructure and the presence of cracks or micro-cracks induced by the effects of corrosion and dynamic loading effects. In previous works [4,5], it was reported that dye penetrants and magnetic particle inspection techniques were effective methods in identifying micro or macro cracks growing from the corroded areas to the parent rail.

Fig. 3 shows the 115-lb/yd and 136-lb/yd rails' microstructures in polished and etched conditions at different magnifications. Both samples show a typical pearlitic steel microstructure along with some non-metallic inclusions inherent to the steelmaking processes. This type of microstructure was observed in both rails and besides the sections with rust all the microstructure looks comparable along the rail. This indicates that corrosion is localized and does not affect the microstructure in areas away from the corroded location. The microscopical inspection did not revealed macro or micro-crack formation in the parent rail material. Therefore, micro-cracks, if any, were considered to have negligible effects on fatigue performance and were not included on the FEA model.

3.3. Finite element analysis (FEA) simulations

Numerical FEA models were conducted using a 115-lb/yd rail and a 136-lb/yd rail. The first FEA model was developed for a 115-lb/yd rail provided by the TTC-Toronto. Fig. 4a–b depicts a highly corroded section of the 115-lb/yd rail showing that

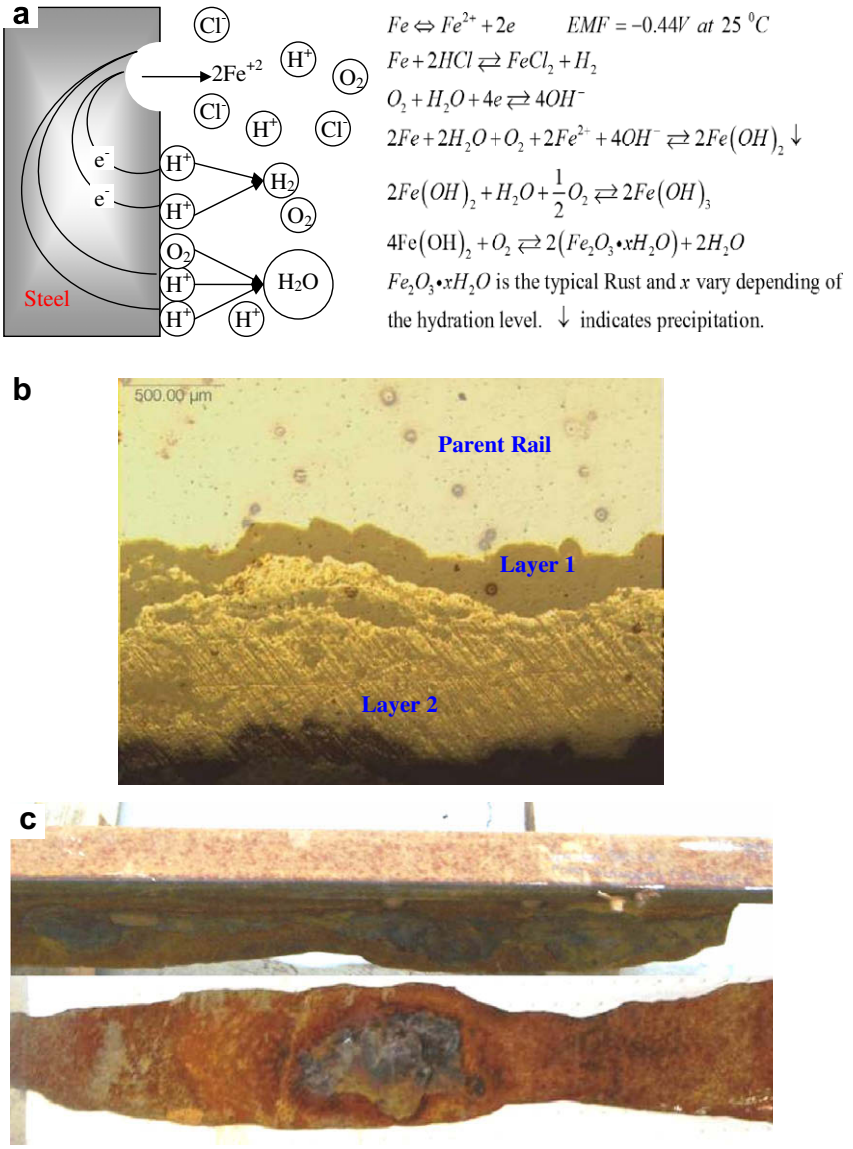

Fig. 2. (a) Electrochemical effects and reactions occurring during corrosion of Fe present in steel in aerated systems containing water (H_2O) and chlorine ions, (b) typical layers observed in rail rust and (c) example of a rail removed from an embedded track.

the structural integrity of the rail was highly compromised. The images in Fig. 4a–b illustrate the challenges associated with detecting rail base corrosion, because this type of corrosion occurs over a tie and is hidden from visual detection except when the flange is corroded and exposes corrosion externally. In addition, some rail flaw vehicle systems have problems to accurately and reliably detect flaws or defects like this at the base of the rail. In contrast other common rail failures can be easily detected either by visual or non-destructive methods [16,17], but in contrast rail base corrosion growth is less unexpected. As a matter of fact, transit authorities reported that in some extreme cases rail base corrosion could not be detected until the rail was removed from track because the corrosion is hidden between the tie and the flanges which is hard area to access with conventional ultrasonic testing methods [4]. In some cases the flange is almost removed leaving behind a thin shell with intact appearance preventing its visual detection.

The other FEA model developed was for a 136-lb/yd rail donated by Amtrak (Fig. 4c). This rail sample was chosen because it is a good example of a common type of corrosion produced by contact between the tie plate and the rail base. In this case, rail base corrosion eroded the rail base evenly leaving behind only a thin section of the rail flange, which in some cases, can be as thin and sharp as a razor blade [4]. Two procedures were used to approximate the effects of corrosion on the base of the 115-lb/yd and 136-lb/yd rails in the FEA simulations. The first procedure used clay moulds to copy the details of the corroded areas and determine the rough dimensions of the corroded area. For the 136-lb/yard rail, a digitized image of the base of the rail (using a FARO-Silver ARM digitizer) was used to get the required information for the FEA model (Fig. 4a and b).

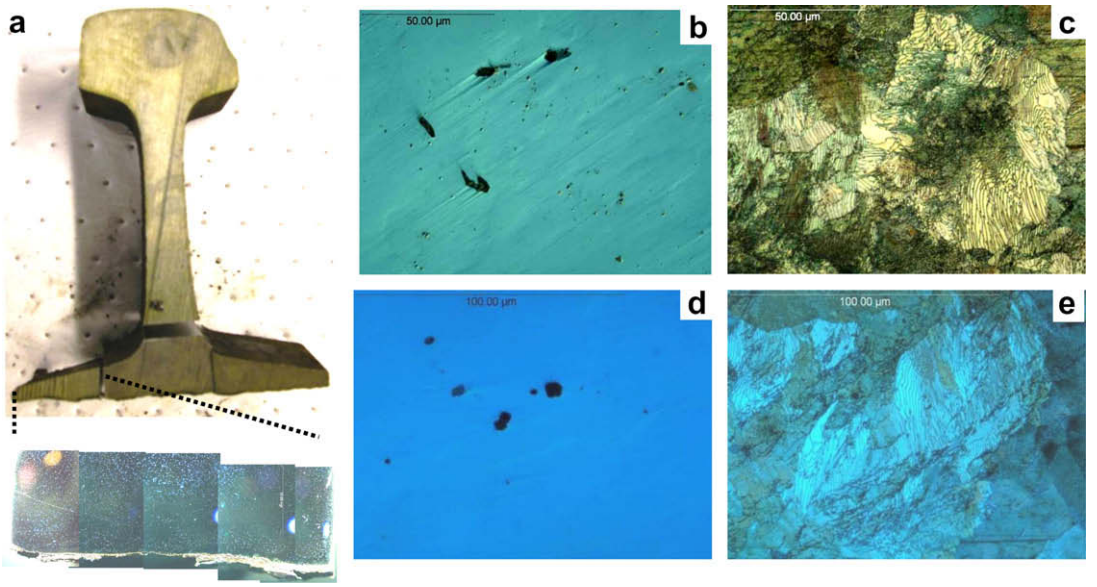

Fig. 3. (a) Picture of a rail cross section and micrographs showing that corrosion does not generate micro-cracks that can growth towards the parent rail, micrographs of the parent rail (b and c) in the vicinity of the corroded section and (d and e) away from the corroded section. Micrographs (a) and (c) are in as polished conditions and (c) and (e) in as etched conditions.

3.4. 115-lb/yd rail FEA

The digitized image was imported into the FEA software (ANSYS) and used to build a highly reliable model that closely represented the characteristics of the corroded rail. The simulation conditions for tie, tie plate dimensions and loads were provided by TTC-Toronto. Fig. 5 shows the results of the FEA simulations. The maximum stresses, due to the stress concentration effects of corrosion, went from 830 MPa to 965 MPa, which is close to and above the yield strength of this steel. This indicates that local yield strength, crack initiation, and crack growth could increase the risk for failure. Locations of highest stress concentration on corroded rails are those having sharp edges as shown in Fig. 5c–d. This can be directly related to stress concentration theory [18].

3.5. 136-lb/yd rail FEA

The typical rail thickness of a 136-lb/yd rail is approximately 1.2 cm. Due to the effects of corrosion (Fig. 5c) the thickness of the rail base for the investigated rail section was reduced to 1.5 mm, such dimension was used in the FEA simulations. Fig. 5e–f shows the results of the FEA simulations for the 136-lb/yd rail. The results of the simulations show maximum stress at the corroded flange was approximately 155 MPa (Fig. 5)e–f. Such stresses are distributed perpendicular to the sharp edge and extend across the width of the rail. This result clearly demonstrates that the maximum stresses in these cases are not as severe as in the previous example. This further confirms that sharp edges are more detrimental than corroded areas that are widely and evenly distributed along the rail base.

3.6. Analysis of finite element simulations

Results from the FEA modeling of the 136-lb/yd and 115-lb/yd rails demonstrate that the type of corrosion found in the 136-lb rail produces less stress concentration than the sharp angles found in the 115-lb/yd rail. The stress concentration is quite dependant on the shape of the corroded sections. Fig. 6 shows the relationship between the size and shape of defects, such as corrosion, and their effect on stress concentration. Fig. 6 can be represented mathematically using Eq. (1) [18].

$$K_t = \frac{\sigma_{MAX}}{\sigma_{NOM}}$$
$$\sigma_{MAX} = \sigma\left(1 + 2\frac{a}{b}\right) \quad (1)$$

where: K_t is the stress concentration factor, a and b are the geometry parameters of cracks, defects, flaws, etc. σ_{MAX} is the maximum stress that results from the stress concentration, σ_{NOM} is the nominal stress or stress applied.

Eq. (1) expresses that stresses are concentrated along the tips of the defects. Eq. (1) shows that as the value of a/b increases, a linear enlargement of the concentration of stresses is observed (e.g., for a circular hole $K_t = 3$). This confirms that

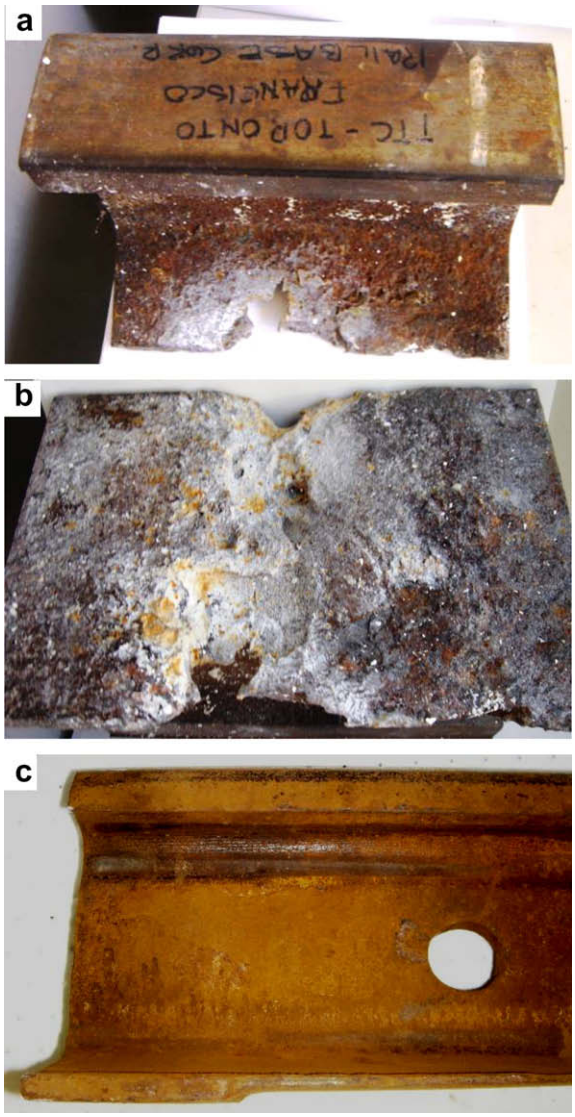

Fig. 4. (a and b) Pictures of a corroded rail on a 115-lb/yd rail and the base of the rail showing intricate corrosion at the base of the rail and (c) pictures of the 136-lb rail showing distributed corrosion along the rail's base.

locations with sharp edges maximize the stresses that are in agreement with the results of the FEA analysis (compare Fig. 5c–f). It is also important to mention that the size and number of defects further contribute to the build up local stresses. However, the sharpness of the flaw is potentially the most detrimental characteristic for stress concentration and can compromise the integrity of the rail significantly. This does not imply that evenly distributed corrosion (Fig. 4 and Fig. 5e–f) does not represent a safety concern. This can be a unique case and for real transit system conditions the presence of intricate shapes are common; this in turn can in real life be worse because corrosion is usually hidden from visual detection under the flanges. The FEA analysis suggests that for the investigated rails the stresses determined along the sharp corner (Fig. 5e–f) are at least seven times larger than the ones shown in Fig. 5e–f.

Corrosion typically causes very intricate defect shapes growing in unpredictable directions and intricate shapes forming sharp angles, which result in significant stress concentration. The analysis of the 115-lb/yd rail demonstrates that the level of stress can be high enough to easily cause failure under the investigated traffic conditions, because the cyclic stresses can reach levels close to or above the yield strength of this steel. Therefore, under this condition the rail can fail under a low cycle fatigue regime. In contrast, the 136-lb/yd rail (Fig. 5e–f) shows that the stresses were considerably below the yield strength of the steel. However, due to the cyclic nature of loading on the transit system, fatigue analysis of this rail was conducted to determine the rail's life under normal traffic conditions. It is important to mention that for this analysis the effects of corrosion rate and growth were not considered in the FEA.

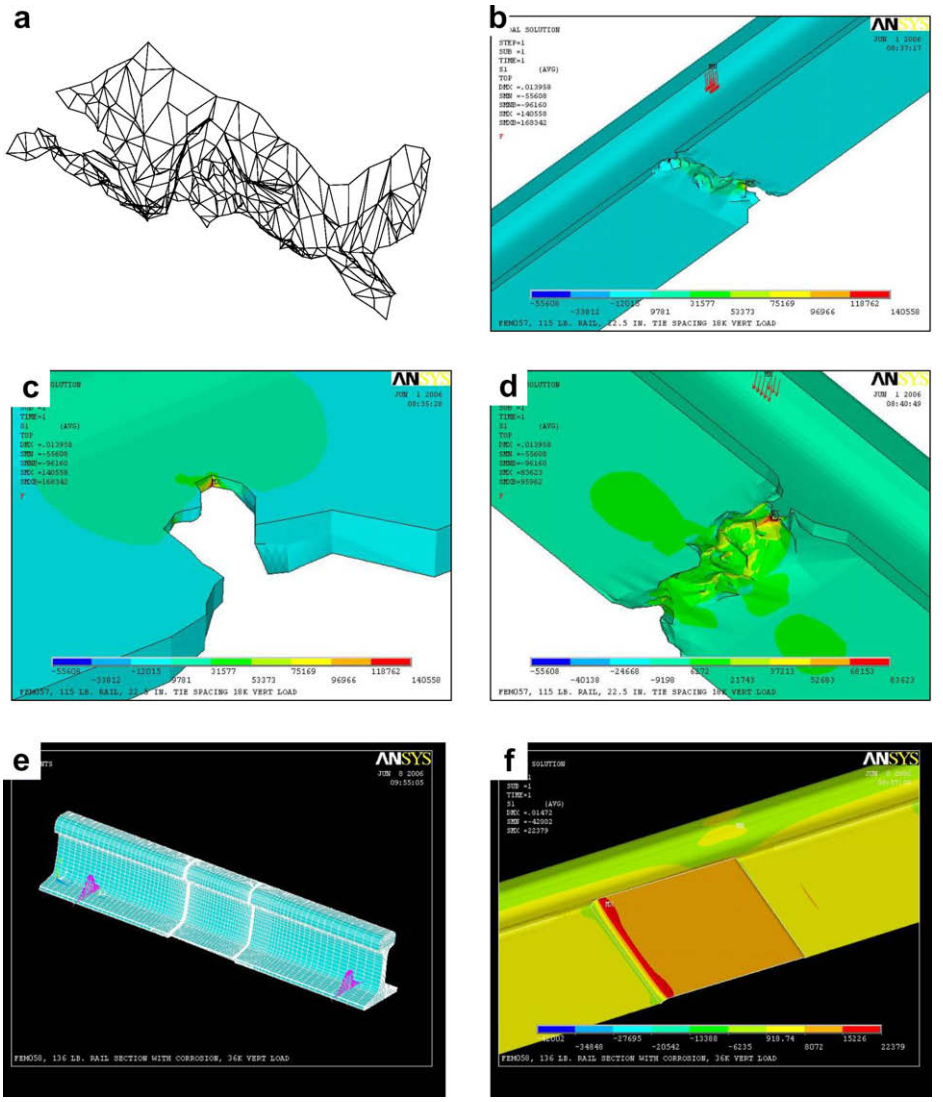

Fig. 5. (a) Digitalized corroded section shown in Fig. 4a and b, (b) digital image of the corrosion inserted at the base of the rail in the FEA mode (c and d) FEA results for the 115-lb rail using the digitalized flaw shown in figures a–b and (e and f) results of the FEA analysis for the 136-lb rail with the corrosion condition shown in Fig. 4c.

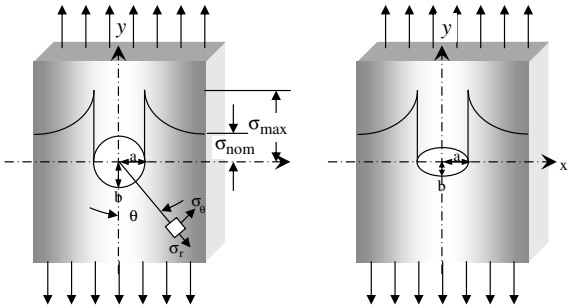

Fig. 6. Stress distribution due to (a) spherical and (b) elliptical holes, respectively, along a component [16].

3.7. High cycle fatigue analysis

The following parameters were used for the high cycle fatigue analysis. The values for the analysis are in accordance to the data provided by Amtrak [4] or the US Department of Transportation [14]:

3.7.1. Load and stress environment

- 216 passenger trains per day.
- Each train contained eight passenger cars and two locomotives.
- Each locomotive weighed 66,000 kg and each car weighed 35,600 kg.
- Wheel loads estimated as 5700 kg for locomotives and 4500 kg for cars.
- FEA was used to calculate maximum stress in corroded areas due to wheel loads.

○ Maximum stresses of 53.5 MPa and 43 MPa for locomotive and passenger car wheel loads were used, respectively. The resulting stress cycle environment used per train consisted of 12 cycles of zero to 53.5 MPa and 32 cycles from zero to 43 MPa.

3.7.2. Rail material properties and fatigue analysis parameters

- A section of the width of a tie was corroded away on the bottom surface of the rail.
- Material is considered to be quenched and tempered wrought steel with yield strength of 827.4 MPa and a tensile strength of about 1180 MPa.
- S–N curve for the material is estimated to have stress range intercept of about 650 MPa and a life cycle of 1.0E6 at 300 MPa. The S–N curve has a constant slope on a Log–Log plot, and the slope remains constant to a life cycle of 1.0E10.
- The S–N curve is considered to be produced from small test samples or coupons, not from full-scale rail samples.
- The Goodman mean stress correction factor was used to account for all cycles having only positive stress.
- A correction factor accounting for a corrosive environment was used to modify the material S–N curve.
- The Miner's constant was reduced from 1.0 to 0.90 to account for the rough surface produced by the corrosion.

3.7.3. Results of the high cycle fatigue analysis

Fig. 7 shows the estimated fatigue life for the 136-lb/yd rail used in the fatigue analysis. In Fig. 7 can be observed that the estimated life (for 50% of the evaluated locations) until crack initiation for the rail shown in Fig. 4 and Fig. 5e–f is approximately 1.39×10^{-7} to 1.87×10^{-7} load blocks or trains. This is equivalent to 176 to 237 years, if there are 216 trains passing through the location each day. This implies that this type of defect is not as dangerous for rails and does not represent a safety concern. However, the corrosion growth was not introduced in the simulations that will reduce the rail's life by increasing the Stress Intensity Factor accelerating the potential to failure considerably. Therefore, by including this effect in the numerical simulation, the rail's life is reduced considerably; this phenomenon is discussed in the following sections.

3.8. Effects of environmental corrosion

After reviewing the plots shown in Fig. 8, it becomes more evident that rails used in different transit systems corroded at a very similar rate, but there is a slight deviation in terms of the voltage drop for every sample. However, the current density

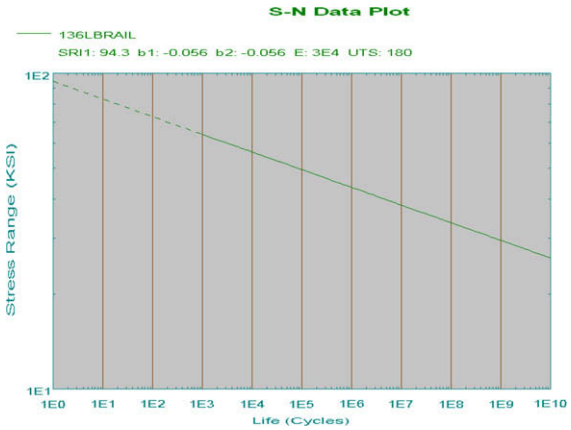

Fig. 7. Simulated S–N Curve for 136-lb rail steel.

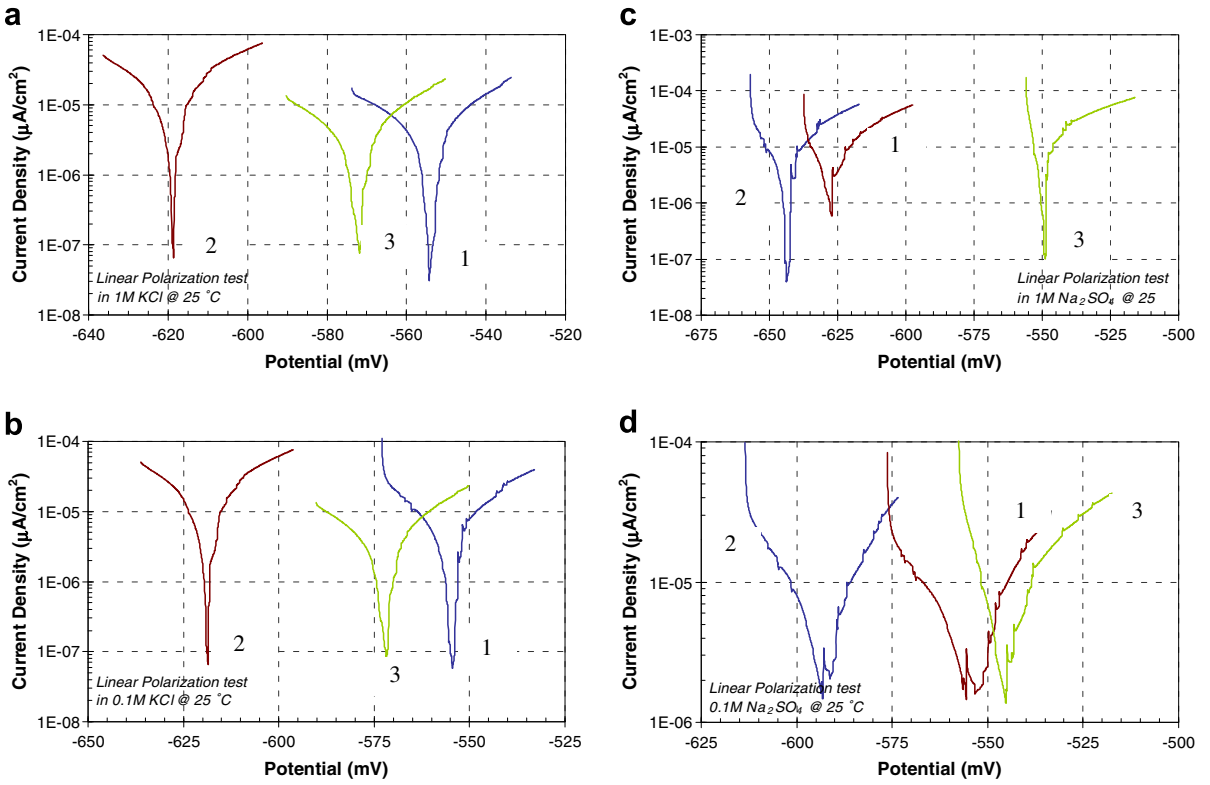

Fig. 8. Corrosion resistance of the different rails in KCl, (a) 1 M KCl electrolyte, (b) 0.1 M KCl electrolyte, Na_2SO_4, (c) 1 M Na_2SO_4 electrolyte and (d) 0.1 M Na_2SO_4 electrolyte.

required for the corrosion of each specimen is in the same order of magnitude. The latter indicates that the materials tested present a similar corrosion resistance regardless of the medium in which they are evaluated (sulfates and chlorines). With the information from Fig. 8, we were able to determine the current density for corrosion. Such current density is found by intercepting the slopes of the anodic and cathodic portions of each plot. Since the current density is directly proportional to the rate of corrosion, we were able to estimate such rate by means of the following equation:

$$r_{\text{corr}} = -\frac{j_0}{nF} \tag{2}$$

where j_0 is the current density for corrosion, n is the number of electrons transferred during the oxidation of the metal and F is Faraday's constant (96500 C/mol). It must be noticed that Eq. (2) expresses the corrosion current as current density. Since there is no net reaction, since the rate of oxidation and reduction within the electrochemical cell are equal. Therefore the exchange reaction is equivalent to either the rate of corrosion or the rate of reduction, thus the corrosion rate can be conveniently expressed in terms of the current density. Thus, the corrosion rate expressed in mm/year was estimated, as seen in Table 1. According to Table 1, it is clear that the corrosion rate of the different samples lies between 0.002 and 0.07 mm/year. From such values it can be said that these materials exhibit excellent corrosion resistance except for the 3 sample tested under 1 M Na_2SO_4 solution, whose corrosion resistance value suggests that in sulfate media this sample only posses fair corrosion resistance.

The data obtained in Table 1, clearly shows that the steel used for this application is able to withstand the attack of different chemicals under normal conditions. In contrast structural highway components have demonstrated to be more sensitive to environmental corrosion that is attributed to the galvanic pair formed among the different components that are in direct contact [23]. If an over voltage is applied to the corroding system, then the rate of corrosion of the steel will increase significantly.

3.9. Plastic ties

Plastic ties have the potential to prevent leaks of stray electric currents traveling from the rails to ground, thereby reducing rail base corrosion. In previous research plastic ties from different manufacturers were evaluated in the field since 1997 by TTCI demonstrating that their performance is comparable to that of the wood ties [21,22]. The first group of ties that were installed in track was subjected to more than 1 million MGT (million gross tons) of heavy axle load traffic at the facility for

Table 1
Rate of corrosion of the different samples in every tested electrolyte

Electrolyte	Sample	*i* corr (A/cm^2)	Corrosion rate (mol/cm^2/s)	Corrosion rate (g/cm^2/h)	Corrosion rate (mm/year)
KCl 1 M	1	2.5×10^{-6}	-8.6×10^{-12}	-1.7×10^{-7}	-1.8×10^{-3}
	2	9.5×10^{-6}	-3.3×10^{-11}	-6.6×10^{-6}	-0.07
	3	2.5×10^{-6}	-8.6×10^{-12}	-1.7×10^{-7}	-1.8×10^{-3}
KCl 0.1 M	1	4×10^{-6}	-1.4×10^{-11}	-2.8×10^{-6}	-0.03
	2	6×10^{-6}	-2.1×10^{-11}	-4.2×10^{-6}	-0.04
	3	3×10^{-6}	-1.0×10^{-11}	-2.1×10^{-6}	-0.02
Na_2SO_4 1 M	1	3.5×10^{-6}	-1.2×10^{-11}	-2.4×10^{-6}	-0.03
	2	5.5×10^{-6}	-1.9×10^{-11}	-3.8×10^{-6}	-0.04
	3	9×10^{-5}	-3.1×10^{-10}	-6.2×10^{-5}	-0.64
Na_2SO_4 0.1 M	1	2×10^{-6}	-7.0×10^{-12}	-1.4×10^{-6}	-0.01
	2	2.5×10^{-6}	-8.6×10^{-12}	-1.7×10^{-7}	-1.8×10^{-3}
	3	3×10^{-6}	-1.0×10^{-11}	-2.1×10^{-6}	-0.02

accelerated service testing. The majority of the plastic ties tested has the same dimensions and weighed about the same as typical hardwood ties.

Laboratory tests conducted to characterize the electrical resistance of plastic ties focus on the determination of their insulating capacity. Fig. 9 shows one of the plastic ties tested indicating the locations where the resistance measurements were taken. The minimum allowable electrical impedance (resistance) of 20 kΩ for concrete crossties, as specified in the AREMA manual for railway engineering, was used as a baseline. Since the plastic ties tested are almost impermeable on their exterior, the test was conducted on cross sectional slices to expose any internal porosity (Fig. 9). The purpose of exposing the porosity was to simulate a worse case condition, where water entered the interior of the tie and potentially increased its electrical conductivity. The electrical resistance was measured under dry and water-soaked conditions (Immersed in water for 3 weeks) the measurements were taken using typical screw spikes and some were taken directly on the surface of the plastic tie. The results indicate that measurement location 1 (Fig. 9), screw spike to screw spike, provided the least resistance in all three tie types. The electric resistance of plastic ties ranges from 5 MΩ/m (250 times higher than the AREMA minimum) to the overload of the ohmmeter. This, to some extend, indicates the potential of plastic ties as insulator to prevent rail base corrosion. However, plastic ties can also be a risk because an insulated track with a small location with a stray current will increase the current density relived resulting in the acceleration of local corrosion effects. In order to minimize the effects of stray currents the rail can be grounded in various locations and the method is discussed in the following sections of this paper.

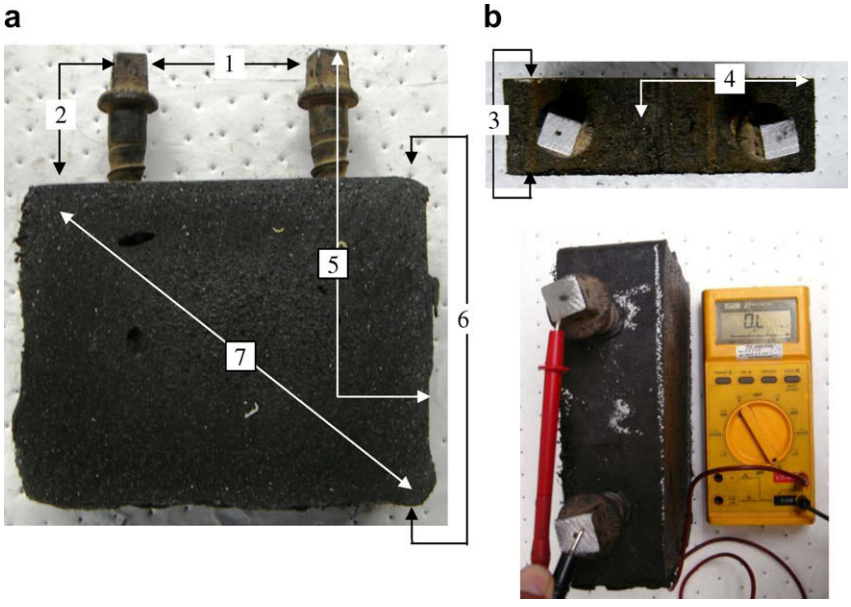

Fig. 9. The electrical resistance measurements were taken at seven locations under dry and water-soaked conditions using a typical ohmmeter. Arrows and numbers indicate the location where the resistance was measured.

4. Discussion

The simplest and most common approaches to determine the amount of material loss can be determined using the Faraday's law and in order to assess the probability of corrosion, the Nernsťs equation (Eq. (3)) [1,19]. Farady's Faraday's (Eq. (4)):

$$E = E_0 - \frac{RT}{nF}\log\frac{a_{\mathrm{Red}}}{a_{\mathrm{Ox}}} = \Delta E = -\frac{RT}{nF}\log\frac{[\text{ion out of the cell}]}{[\text{ion out of the cell}]} \tag{3}$$

where E is the equilibrium reduction potential and E_0 is the standard reduction potential, R is the gas constant, T is the temperature in Kelvin, n is the number of electrons transferred in half the reaction, F is the Faraday's constant (9.7×10^{-4} °C/mol), a_{Red} and a_{Ox} are the respective reduction and oxidation activities.

$$\begin{aligned} &F = N_{Aq} \\ &m = \frac{Q}{q\cdot n}\cdot\frac{M}{N_A} = \frac{1}{192970}\cdot\frac{QM}{\eta} \\ &\eta_{Fe} = 2.\therefore \\ &m = 5.1822 \times 10^{-6}\cdot QM \end{aligned} \tag{4}$$

where F is the Faraday constant, N_A is the Avogadro's number (6×10^{23} ions/mol), m is the mass of the substance produced or lost during electrolysis, Q is the total electric charge passing through the system, q is the electron charge (1.6×10^{-19} coulombs per electron), η is the valence of the substance in solution and M is the molar mass of the substance in grams/mol. To remove 1 mol of material is required 1 Faraday by the valence of such element. The total charge for electrolysis is as follows:

$$Q = \int_0^T I(t)\mathrm{d}t = I\cdot t \tag{5}$$

In the transit systems the voltage required to initiate the electrochemical reaction for iron is −0.44 VDC. The return voltage from the locomotive to the rail in the North American transit systems is from 400 V to 1000 V. Therefore, rails under these conditions are definitely undergoing corrosion at the base of the rail in the presence of stray currents. For this electrolytic-like system the tie plate is the cathode and the rail is the anode; a scheme is presented in Fig. 10. Stray currents are created due to the fact that current will tend to travel along all the paths to return to the power station. Therefore, any path that closes the circuit will be used for the DC current to return to the power station. The amount of current that strays is proportional to the ratio in resistance among the various paths as shown in Eq. (6) [6].

$$I_{\mathrm{Stray}} = \frac{Ir_t l^2}{8r_c} \tag{6}$$

where I is the traction current in A, r_t is the resistance of the track in Ω/km, l is the distance between the train and the substation in km, and r_c is the resistance between the rail and ground. The return current density along the 115-lb/yd and 136-lb/yd rails are given in Table 2. From Table 2 it can be observed that the current density that returns along the rails is relatively low even for the hypothetical case in which the return current is 1000 A.

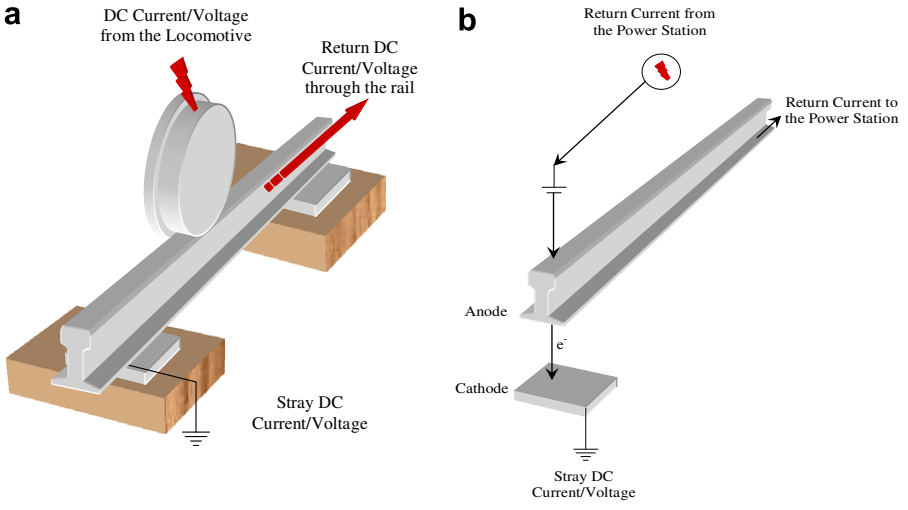

Fig. 10. Electrical configuration of the (a) locomotive/rail/tie plate/ground and (b) electrolytic system formed among the above mentioned components.

Table 2
Current densities for ll5-lb/yd and 136-lb/yd rail profiles

Rail Type (lb/yd)	Surface area		Returned current density (A/cm^2)		
	in^2	cm^2	1 A	600 A	1000 A
115	10.5	67.74	0.0148	8.857	14.76
136	13.5	87.097	0.0115	6.889	11.48

The average electrical resistance of rail steel is 96.1 nΩ/m. In contrast, 30 Ωm and 180 Ωm are the common values of electrical resistance for wet and dry grounds [3,6]. Fig. 11 shows the calculated stray currents and weight of rail lost per year for different stray currents levels and for trains located at different locations with respect to the power station. Fig. 11 was determined for rails under normal conditions and rails with insulated plastic ties. Stray currents were determined using Eq. (6) and the amount of rail lost was determined using Eq. (4). The amplitude of the return current (1 A, 600 A and 1000 A) used

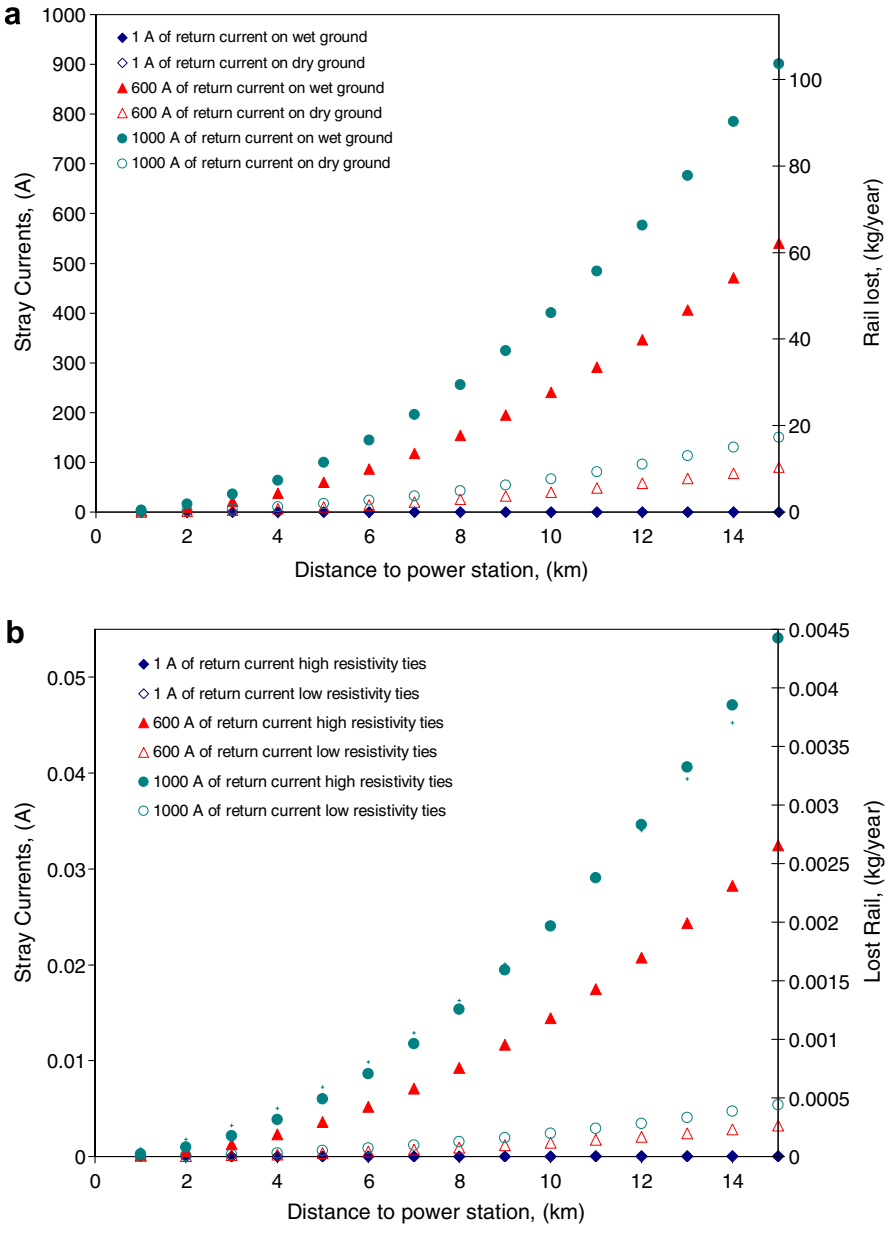

Fig. 11. Stray currents and rail lost for (a) wood and (b) plastic ties.

in Fig. 11 are hypothetical values to illustrate the effect of the magnitude of the stray current on corrosion. The calculations indicate that approximately 6.5 kg of rail·km^{-1} year^{-1} (>0.05%) is not a large amount; however, rail base corrosion is a localized issue (as seen in Figs. 2–4); therefore its effects can be detrimental. In fact, 6.5 kg is equivalent to the removal of approximately 5.2 cm and 4.4 cm of the entire cross section of the rail for the respective 115-lb/yd or 136-lb/yd rails. Or the entire base and flanges of the rail in a length of approximately 60–75 cm (for the 136 and 115-lb/yd, respectively). If the ratio in resistance between the rail and ground is further reduced the corrosion effect will increase accordingly; therefore, a potential way to prevent corrosion is by insulating material such as plastic ties.

The use of plastic ties can result in significant reduction of rail lost material as seen in Fig. 11b. The reduction of the rail base lost due to corrosion is at least 30,000 times larger for rails insulated with plastic ties when compared to non-insulated wood or concrete ties. Unfortunately, insulation can also be detrimental, because in the case that a location presents stray current then a high current density will be transmitted along this spot. In addition, electrical continuity of the rail promotes proper return DC current supporting the electrical continuity and conductivity for the return of the current. Therefore, introducing plastic ties as insulation for stray current needs to be accompanied by the use of a controlled stray current system (ground the rails at various locations). This can release excessive current at a particular location resulting in a reduction of the stray DC current reducing its current density and hence corrosion potential. The ground system should be connected and used as a second return current system preventing further damage to neighbor electric systems such as city structures and drainage.

5. Conclusions

Rail base corrosion can considerably shorten rail's life and be a potential cause of failure due to the affects of fatigue and fatigue-corrosion. Rail base corrosion locally affects rail steel in areas where corrosion is present but has negligible effects to the rest of the rail. The corrosion rate along the rail base is affected by humidity and deposited salts but most importantly by stray DC currents that generate electrolytic reactions. Electrolytic reactions increase galvanic corrosion effects and corrosion rates considerably. However, salts (sulfates and chlorines) itself in the absence of stray DC currents do not represent a major concern for rails. The results of the FEA analysis indicate that intricate shapes, in particular sharp angles, are more detrimental to the rail's integrity than the overall size of the corroded region. Proper insulation combined with a stray DC currents control system will prevent rail base corrosion considerably. Perhaps the amount of rail lost due to corrosion effects is relatively low (<0.005%); but since this is a localized effect that forms intricate-unpredictable shapes this represent a serious concern for rail's integrity shortening rail's life and compromising safety.

Acknowledgements

TTCI acknowledges the National Academies, in particular the Transit Cooperative Research Program (TCRP), for providing outstanding support to this project. TTCI also thanks those in the transit industry who responded to the survey on "Practices and Problems associated with Rail base Corrosion." TTCI expresses gratitude to the personnel that assisted during site visits to the various transit locations and to those who provided corroded rail samples for this study. A special acknowledgement goes to Dr. Dingqing Li and Mr. Robert Florom at TTCI for their professional guidance and excellent support during the project. Finally, FCRH would like to thank Mr. Rafael Jimenez and Mr. Gregory. Garcia for their invaluable help and for sharing his knowledge on corrosion, plastic ties, non-destructive testing, respectively and for providing key reference literature. Thanks are also to the Materials Department from the UAM-Azcapotzalco for their assistance with the corrosion tests.

References

[1] Fontana MG, Greene ND. Corrosion engineering, materials science and engineering series, 1985. London: McGraw-Hill; 1978.
[2] Roberge PR. Handbook of corrosion engineering. McGraw-Hill; 2000.
[3] Stray Currents in Transit Systems, www.corrosion-doctors.org/StrayCurrent/Transit-Systems.htm [as posted on 07.21.06].
[4] Robles Hernandez, FC, Koch K, Plascencia Barrera G, Rail base corrosion detection and prevention TCRP web document http://onlinepubs.trb.org/onlinepubs/tcrp/tcrp_webdoc_37.pdf, 2007.
[5] Robles Hernández FC, Koch K, Rail base corrosion analysis: a major factor that shortens the service life of rail in North American transit systems. 136 TMS Annual Meeting and Exhibition, Orlando, FL; 2007.
[6] Cotton I, Charalambous C, Aylott P, Ernst P. Stray current control in the DC mass transit system. IEEE Trans Vehicle Technol 2005;5(4):2.
[7] Chen SL, Hsu SC, Tseng CT, Yan KH, Chou HY, Too TM. Analysis of rail potential and stray current for Taipei metro. IEEE Trans Vehicle Technol 2006;55(1).
[8] Carpenter DC, Hill RJ. Railroad track electrical impedance and adjacent track crosstalk modeling using finite-element analysis method of electromagnetic system analysis. IEEE Trans Vehicle Technol 1993;42:4.
[9] Mariscotti A, Pozzobon P. Experimental results on low rail-to-rail conductance values. IEEE Trans Vehicle Technol 2005;54:3.
[10] Kristan J. FAST Rail evaluation test – fracture performance and discussion. Technology Digest, TD05-024, AAR-TTCI, 2005;1.
[11] American Railway Engineering and Maintenance-of-the-Way Association Chapter IV, Rail Specifications 4-2-1, 2006.
[12] CORPRO Canada Inc., Corrosion protection study, Edmonton Light Rail Train System (041212-102A), Stantec Consulting Ltd., Edmonton, AL Canada; 2005.
[13] TCRP Report 57 Track design handbook for light rail transit, Chapter 8: Corrosion Control, Federal Transit Administration, Transportation Research Board and the National Research Council; 1999.
[14] US Department of Transportation Federal Railroad Administration High Speed Ground transportation for America, Washington DC, USA; 1997.
[15] AREMA, Electrical resistance test, Manual for Railway Engineering, 1, Article 1.9.1.14, 2005.
[16] Beretta S, Boniardi M, Carboni M, Desimon H. Mode II fatigue failures at rail butt welds 2005;12:157.

[17] Mutton PJ, Alvarez EF. Failure modes in alumni thermic rail welds under high axle load conditions 2004;11:151.
[18] Dieter GE. Mechanical metallurgy. McGraw Hill; 1976.
[19] Callister WD. Materials science and engineering an introduction. 7th ed. John Willey and Sons; 2007.
[21] Rafael J, Davis D. In-track performance of plastic composite ties under heavy axle loads at FAST, TD-06-015, AAR-TTCI; 2006.
[22] Rafael J, Davis D, LoPresti J. Progress report: in-track performance of plastic composite ties at FAST, TD-02-004, 2002.
[23] Deflorian F, Rossi F. Premature corrosion failure of structural highway components made from weathering steel. 2002;9:541.